

Theoretical model for scattering of radar signals in K_u - and C-bands from a rough sea surface with breaking waves

A G Voronovich¹ and V U Zavorotny

NOAA/Environmental Technology Laboratory, 325 Broadway, Boulder, CO 80305, USA

E-mail: alexander.voronovich@noaa.gov

Received 26 March 2001

Abstract

A small-slope approximation (SSA) is used for numerical calculations of a radar backscattering cross section of the ocean surface for both K_u - and C-bands for various wind speeds and incident angles. Both the lowest order of the SSA and the one that includes the next-order correction to it are considered. The calculations were made by assuming the surface-height spectrum of Elfouhaily *et al* for fully developed seas. Empirical scattering models CMOD2-I3 and SASS-II are used for comparison. Theoretical calculations are in good overall agreement with the experimental data represented by the empirical models, with the exception of HH-polarization in the upwind direction. It was assumed that steep breaking waves are responsible for this effect, and the probability density function of large slopes was calculated based on this assumption. The logarithm of this function in the upwind direction can be approximated by a linear combination of wind speed and the appropriate slope. The resulting backscattering cross section for upwind, downwind and cross-wind directions, for winds ranging between 5 and 15 m s⁻¹, and for both polarizations in both wave bands corresponds to experimental results within 1–2 dB accuracy.

1. Introduction

Continuous monitoring of the wind over vast ocean areas by remote sensing is essential for weather forecasting. Airborne and satellite microwave scatterometers are the key remote-sensing instruments used to determine the near ocean-surface wind vector. The basic idea of the technique relies on the assumption that the ocean surface normalized radar cross section (NRCS) is correlated with the local surface wind speed and direction. Wind retrieval from radar scatterometry was developed based on existing data sets of collocated contact and scatterometric measurements. The assumption of a strong correlation between the surface wind vector and the surface NRCS works well for moderate and uniform winds, and explains the

¹ Author to whom correspondence should be addressed.

success of various empirical geophysical model functions (GMFs) such as SASS-II, CMOD2-I3 and NSCAT2, all of which use this assumption [1–8]. However, backscattering depends on the previous history of the wind and wave fields, wave age, fetch, wind variability, atmospheric stability and other parameters, as well as on the electromagnetic wavelength λ and angles of observation [9–13]. Recent airborne scatterometer experiments show that these models fail at high wind speeds, especially in hurricane conditions where current GMFs significantly over-predict the NRCS sensitivity to ocean surface wind speed and direction [14, 15]. As a result, satellite scatterometers underestimate the true surface wind field for high wind-speed events. In view of the large number of parameters involved, the best solution of the inverse problem cannot be one that relies on purely empirical relations between scattering and environmental data.

Thus, it is necessary to calculate the scattering cross section from a sea with a given spectrum and statistics of the rough surface. This is often accomplished using a two-scale (composite-surface) model [16–29]. This model introduces a scale-dividing parameter k_d separating small- and large-scale components of the roughness which can be arbitrarily chosen within wide limits. There are therefore two terms in the NRCS. The first one corresponds to the Kirchhoff solution for the large-scale component (specular reflections), and the second one corresponds to the Bragg scattering solution for the small-scale component modulated by tilts of large-scale waves.

This model, however, suffers from two inherent drawbacks. Different authors make different choices for the parameter k_d which range from $k/1.5$ to $k/40$ (see, e.g., table 2 in [30]): Wentz [17] $k_d = \lambda/1.5$; Brown [18], Thompson [24] $k_d = k/3$; Durden and Vesecky [21] $k_d = k/5$; Jackson *et al* [30] $k_d = k/3$ to $k_d = k/6$; Plant [22] $k_d = k/5$ to $k_d = k/10$; Donelan and Pierson [23] $k_d = k/40$; where $k = 2\pi/\lambda$ is the electromagnetic wavenumber. The dependence of this parameter on the grazing angle and/or wind (if any) can be introduced using various guidelines. It is usually claimed that the dependence of the results on the choice of k_d is weak; however, quantitative support of this statement is rarely provided. Secondly, the two-scale model does not allow the evaluation of the effect of higher-order corrections on its results. Hence, the accuracy of the calculations cannot be estimated.

As a result, it remains generally unclear whether the differences between theoretical calculations and experimental data should be attributed to deficiencies of the scattering model or to the inaccurate description of sea roughness. In addition, occasionally the authors invoke modifications of the original models of the sea roughness spectrum used in their calculations to achieve better correspondence between their theoretical calculations and the experimental data. The issue of consistency of the modifications with pertinent hydrodynamic data is rarely addressed. In order to take into account the loss of reflected power in a near-nadir direction due to the ripples on large waves, the local Fresnel reflection coefficient is often multiplied in the Kirchhoff solution by an empirically derived coefficient close to 0.65 [29].

In this paper we present scattering calculations based on the small-slope approximation (SSA) [31, 32], which does not have the above-mentioned drawbacks. It does not invoke any arbitrary parameters. For the Gaussian statistics of roughness, the result can be expressed strictly in terms of a roughness spectrum. The SSA can be applied to an arbitrary wavelength, provided the tangent of grazing angles of incident/scattered radiation sufficiently exceeds RMS slopes of roughness. The SSA represents a regular expansion of the scattering amplitude (or the scattering cross section) in terms of the roughness slope, and both the first- and the second-order results of SSA calculations can be obtained. When the difference between the first- and the second-order results is relatively small, one can be sure that the solution of the scattering problem is accurate. This removes doubts concerning the solution of the

electrodynamic part of the problem. It can be proven that the effect of modulation of scattering by tilted facets (the basic concept of the two-scale model) is correctly taken into account by the SSA [33].

In our simulations we used the Elfouhaily *et al* model [34] for the sea roughness spectrum, which was recently developed based on available field and wave-tank measurements, along with physical arguments. It is important to note that this model was developed without any relation to remote-sensing data. We avoided some deficiencies of this spectral model found in [27]. We calculated the backscattering cross section for K_u - ($\lambda = 2.14$ cm) and C-bands ($\lambda = 5.45$ cm) as a function of incidence angle for up-, down- and cross-wind directions for three wind speeds $U = 5, 10$ and 15 m s⁻¹. Averaged experimental data for K_u - and C-bands were provided by SASS-II [3] and CMOD2-I3 [7] empirical models that were developed based on extensive data sets obtained during ERS-1 and SASS missions. The SASS-II model was also confirmed by comparisons with airborne measurements [14, 15].

In general, the theoretical and experimental results appear to be in good agreement, with an average absolute error within 1–2 dB. However, there is a significant underestimate of the order of 5–6 dB of the backscattering cross section for HH-polarization, σ_{HH} , for relatively large incidence angles in the upwind direction. The mismatch significantly exceeds the accuracy of our calculations, the maximal value of which is of the order of 2 dB (see section 3 below). This underestimate is typical for most of the numerical simulations. We attribute the difference to the effect of a relatively small percentage of steep breaking waves. Using this assumption we were able to calculate the physically reasonable probability density of large slopes which are beyond the ranges of validity of the Cox–Munk distribution [35, 36].

The paper is organized as follows. In section 2 a brief derivation is given of the expressions for the scattering cross section according to the SSA of the first and second order. In section 3 we present results of numerical simulations and comparisons with the model function derived from experimental data. In section 4 we suggest a modification of the sea-roughness model which includes the effect of steep waves. Finally, in section 5 the results are discussed and conclusions are drawn.

2. Scattering cross section in the small-slope approximation

The small-slope approximation is appropriate for scattering from both large- (the Kirchhoff regime), intermediate- and small-scale (the Bragg regime) roughness within a single theoretical scheme. The SSA can be applied for an arbitrary wavelength, provided the tangent of grazing angles of incident/scattered radiation sufficiently exceeds the RMS slopes of roughness. The slopes of sea-surface roughness are generally small except for steep breaking waves which comprise a relatively small percentage. Another advantage of the SSA is that it represents regular expansion with respect to powers of slope. Thus, both the lowest-order approximation (which we refer to as the SSA-1) and the next-order approximation (the SSA-2), which includes corrections to the SSA-1, can be calculated. The SSA was successfully used for interpretation of experimental data in ocean acoustics [37], and was verified in a number of numerical simulations [38–41].

To calculate statistical characteristics of scattering using the SSA one must know the characteristic functions of the random field of elevations. These characteristic functions for sea-surface roughness are unknown. However, for Gaussian statistics they can be expressed through a correlation function of roughness. It will be assumed that the background sea-surface roughness obeys Gaussian statistics, whereas the deviation from Gaussianity (in our case, skewness) will be assumed to be small and attributed to a small percentage of steep breaking waves. Because the large slopes of steep waves would not be amenable to the SSA,

we cannot use this theory for calculations of backscattering from such waves. This will be done separately based on the geometric optics limit of the Kirchhoff approximation.

The SSA presents an explicit expression for the scattering amplitude (SA) $S(\vec{k}, \vec{k}_0)$ on the basis of plane waves in terms of parameters of the incident and scattered waves and surface roughness elevations $h(\vec{r})$ [32]:

$$S(\vec{k}, \vec{k}_0) = \frac{2(q_k q_0)^{1/2}}{q_k + q_0} \int \frac{d\vec{r}}{(2\pi)^2} \exp[-i(\vec{k} - \vec{k}_0)\vec{r} + i(q_k + q_0)h(\vec{r})] \times \left(B(\vec{k}, \vec{k}_0) - \frac{i}{4} \int M(\vec{k}, \vec{k}_0; \vec{\xi}) \widehat{h}(\vec{\xi}) \exp(i\vec{\xi}\vec{r}) d\vec{\xi} \right). \quad (1)$$

In equation (1) $\vec{r} = (x, y)$ are horizontal coordinates and \vec{k}_0 and \vec{k} are horizontal projections of the wavevector of incident and scattered waves, correspondingly, and

$$\widehat{h}(\vec{\xi}) = \int h(\vec{r}) \exp(-i\vec{\xi}\vec{r}) \frac{d\vec{r}}{(2\pi)^2} \quad (2)$$

is a Fourier transform of h . Values $-q_0$ and q_k are appropriate vertical projections of the wavevectors:

$$q_0 = \sqrt{\frac{\omega^2}{c^2} - k_0^2} \quad q_k = \sqrt{\frac{\omega^2}{c^2} - k^2} \quad \text{Im } q_0, q_k \geq 0 \quad (3)$$

and

$$M(\vec{k}, \vec{k}_0; \vec{\xi}) = B_2(\vec{k}, \vec{k}_0; \vec{k} - \vec{\xi}) + B_2(\vec{k}, \vec{k}_0; \vec{k}_0 + \vec{\xi}) + 2(q_k + q_0)B(\vec{k}, \vec{k}_0). \quad (4)$$

SA $S(\vec{k}, \vec{k}_0)$ represents a 2×2 matrix describing mutual transformations of the electromagnetic (EM) waves of different polarizations. Namely, $S_{\alpha\alpha_0}(\vec{k}, \vec{k}_0)$ is an amplitude of scattering of an incident plane wave characterized by the horizontal wavevector \vec{k}_0 and polarization $\alpha_0 = 1, 2$ into a scattered plane wave with horizontal wavevector \vec{k} and polarization $\alpha = 1, 2$. In our case the polarization index $\alpha = 1$ corresponds to a conventionally defined vertical polarization, and $\alpha = 2$ corresponds to a horizontal polarization. Values B , B_2 and M are 2×2 matrices. Explicit expressions for these matrices on the basis of vertically and horizontally polarized waves are reproduced for the reader's convenience in the appendix. One can see that the entries of these matrices are regular complex functions of their arguments that can be easily calculated.

It can be proven [42] that in a general case $M(\vec{k}, \vec{k}_0; 0) = 0$, and for this reason the term related to the function M in equation (1) is, in fact, proportional to the slopes of roughness rather than to the elevations themselves. This term provides a correction to the SSA-1. Thus, equation (1) corresponds to the SSA-2, and using $M = 0$ in it results in the lowest-order approximation, the SSA-1. A detail derivation of the SSA in the general case can be found in [31], and in the EM case specifically in [32].

The expression for a scattering cross section is directly related to the second-order statistical moment of the SA [31, 32]. The simple calculation for the SSA-1 yields the following expression for a dimensionless scattering cross section $\sigma_{\alpha\alpha_0}$ for scattering of the wave of polarization α_0 into the wave of polarization α :

$$\sigma_{\alpha\alpha_0}(\vec{k}, \vec{k}_0) = \frac{1}{\pi} \left| \frac{2q_k q_0}{q_k + q_0} B_{\alpha\alpha_0}(\vec{k}, \vec{k}_0) \right|^2 \exp[-(q_k + q_0)^2 W(0)] \times \int \left\{ \exp[(q_k + q_0)^2 W(\vec{r})] - 1 \right\} \exp[-i(\vec{k} - \vec{k}_0)\vec{r}] d\vec{r}. \quad (5)$$

According to the above-mentioned meaning of polarization indices, $\sigma_{VV} = \sigma_{11}$ and $\sigma_{HH} = \sigma_{22}$. Here, function $W(\vec{r})$ is defined by the relation

$$\langle \exp [iQ (h(\vec{r}_1) - h(\vec{r}_2))] \rangle = \exp [-Q^2 (W(0) - W(\vec{r}_1 - \vec{r}_2))] \quad (6)$$

and the condition $W(\vec{r}) \rightarrow 0, \vec{r} \rightarrow \infty$. Here, $\langle \cdot \rangle$ means averaging over the space-homogeneous statistical ensemble of sea-surface roughness. For Gaussian statistics W represents the correlation function of roughness; in a general case equation (6) can be viewed as a definition of function W .

To facilitate calculations in the case of the SSA-2 first we perform the following transformation:

$$B_{\alpha\alpha_0}(\vec{k}, \vec{k}_0) - \frac{i}{4} \int M_{\alpha\alpha_0}(\vec{k}, \vec{k}_0; \vec{\xi}) \widehat{h}(\vec{\xi}) \exp(i\vec{\xi}\vec{r}) d\vec{\xi} \\ \approx B_{\alpha\alpha_0}(\vec{k}, \vec{k}_0) \exp \left[-\frac{i}{4B_{\alpha\alpha_0}(\vec{k}, \vec{k}_0)} \int M_{\alpha\alpha_0}(\vec{k}, \vec{k}_0; \vec{\xi}) \widehat{h}(\vec{\xi}) \exp(i\vec{\xi}\vec{r}) d\vec{\xi} \right]. \quad (7)$$

Since the second term on the left-hand side of equation (7) should represent a small correction to the first one, such an approximation (suggested first in [43]) is legitimate. Using equation (7) in equation (1) we see that the SSA-2 reduces to the SSA-1 when $h(r)$ is substituted by modified roughness $h_M(\vec{r})$:

$$h_M(\vec{r}) = \int \left(1 - \frac{M_{\alpha\alpha_0}(\vec{k}, \vec{k}_0, \vec{\xi})}{4(q_k + q_0)B_{\alpha\alpha_0}(\vec{k}, \vec{k}_0)} \right) \widehat{h}(\vec{\xi}) \exp(i\vec{\xi}\vec{r}) d\vec{\xi}. \quad (8)$$

The modified roughness depends on \vec{k}, \vec{k}_0 and can be a complex value. For Gaussian statistics of elevations $h(\vec{r})$, the modified roughness $h_M(\vec{r})$ is also a Gaussian value, and averaging of the correlator entering the expression for the scattering cross section yields

$$\langle \exp [iQ (h_M(\vec{r}_1) - h_M^*(\vec{r}_2))] \rangle = \exp \left[-\frac{Q^2}{2} (\langle h_M^2 \rangle + \langle h_M^2 \rangle^* - 2W_M(\vec{r}_1 - \vec{r}_2)) \right] \quad (9)$$

where

$$W_M(\vec{r}) = \langle h_M(\vec{\rho} + \vec{r}) h_M^*(\vec{\rho}) \rangle \\ = \int \left| 1 - \frac{M_{\alpha\alpha_0}(\vec{k}, \vec{k}_0, \vec{\xi})}{4(q_k + q_0)B_{\alpha\alpha_0}(\vec{k}, \vec{k}_0)} \right|^2 S(\vec{\xi}) \exp(i\vec{\xi}\vec{r}) d\vec{\xi} \quad (10)$$

where $S(\vec{\xi})$ is the spectrum of roughness:

$$W(\vec{r}) = \int S(\vec{\xi}) \exp(i\vec{\xi}\vec{r}) d\vec{\xi}. \quad (11)$$

Since we will no longer be using scattering amplitude $S(\vec{k}, \vec{k}_0)$, this notation will not lead to confusion. It is easy to see that to first-order accuracy with respect to M

$$\langle h_M^2 \rangle + \langle h_M^2 \rangle^* \approx 2W_M(0). \quad (12)$$

Thus, calculation of the scattering cross section according to the SSA-2 is reduced to calculation of σ according to the SSA-1, but with a modified spectrum of roughness:

$$S_M(\vec{\xi}) = \left| 1 - \frac{M_{\alpha\alpha_0}(\vec{k}, \vec{k}_0, \vec{\xi})}{4(q_k + q_0)B_{\alpha\alpha_0}(\vec{k}, \vec{k}_0)} \right|^2 S(\vec{\xi}). \quad (13)$$

Note that the modified spectrum S_M is not generally an even function of $\vec{\xi}$.

Numerical evaluation of the integral in equation (5) was implemented as follows. For sufficiently short electromagnetic waves the area on the \vec{r} -plane that is significant for calculation of the integral is concentrated around the origin $\vec{r} = 0$ and is relatively small. It ranges from 0.4 to 1.0 m in diameter for K_u - and C-bands; the size increases both with increasing wavelength and decreasing wind. Within this area we introduce a sufficiently dense, uniform in polar coordinates, web-like net (usually with approximately $10^2 \times 10^2$ nodes) and calculate the function W in all nodes of the net according to equation (11). In the case of the SSA-2, spectrum S is replaced by a modified spectrum S_M and W is replaced by W_M . To calculate the integral in equation (5) we first divide each quadrangle of the net into two triangles. Within each triangle we interpolate W by a linear function of \vec{r} . Thus, throughout the area of integration, W is approximated by a piecewise linear continuous function of \vec{r} . The integral over each triangle can be evaluated using explicit formulae and the calculation of the integral is made quickly.

Calculation of W (or W_M) is accomplished using the same pattern since equation (11) reduces to an integral of equation (5) type when the representation $S = \exp(\log(S))$ is used. The only difference is that to build an appropriate net on the \vec{k} -plane we apply a uniform step with respect to $\log(k)$ rather than to k . Since W should be evaluated at a large number of points \vec{r} , this calculation uses an overwhelming portion of the overall computation time. This time depends on the number of nodes of the web on the \vec{k} -plane (i.e. on the accuracy of the approximation of the roughness spectrum).

When calculation of the scattering cross section is performed according to the SSA-1, the function W must be evaluated for a given roughness spectrum only once, and then σ can be calculated for different incidence/scattering angles quickly. However, when the SSA-2 is used, the modified spectrum S_M in equation (13) depends on \vec{k} , \vec{k}_0 , and the calculation of W_M must be repeated for each new incidence and/or scattering angle, which makes numerical simulations much more extensive.

3. Comparison with experimental data

Before demonstrating the correspondence between SSA calculations and the combination of the geometric optics and the two-scale method, we would like to dwell on the angular dependence of a radar cross section obtained using these traditional methods. It is presented in figures 1(a)–(d) for the K_u -band case. The geometric optics describes the radar cross section for sufficiently small incident angles, whereas the two-scale method covers an area of large incident angles. Figures 1(a) and (c) show a comparison between various curves provided by geometric optics/two-scale model calculations for two polarizations and three values of spectral dividing parameters k/k_d at wind speed $U_{10} = 15 \text{ m s}^{-1}$. It is seen that geometric optics results are sensitive to the value of the spectral dividing parameter. We should point out that even with a reasonable choice of k/k_d these methods have two areas of discrepancy with experimental data. First, the geometric optics result used in the near-nadir direction overestimates data by several dB. As previously noted, the empirically derived ‘effective’ reflection coefficient [29] is frequently used to improve the geometric optics result. Second, there is a region over incidence angles between about 20° and 30° , where two asymptotic curves intersect and none of these approximations is accurate.

Vandemark *et al* [45], suggest that the above-mentioned deviation in the near-nadir cross section results from using a Gaussian statistics of surface slopes in the geometric optics model. They invoke a non-Gaussian slope peakedness to lower the near-nadir cross section and to extend the geometric optics result toward the region of 20° – 30° incidence angles, so the corresponding scattering cross section better fits the measured data.

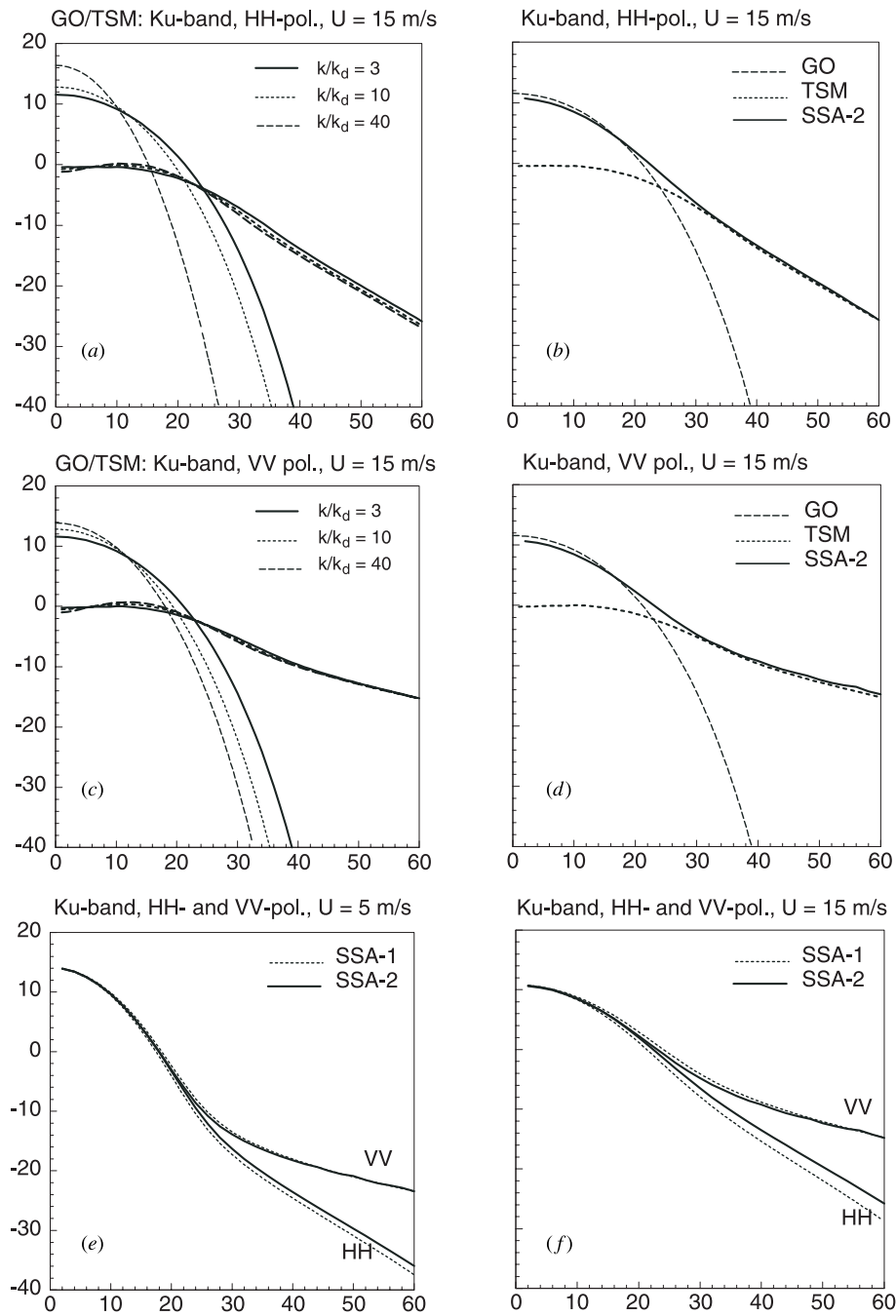


Figure 1. The case of a radar cross section in the K_u -band. (a), (c) Comparison of geometric optics/two-scale model calculations for various values of spectral dividing parameters k/k_d at wind speed $U_{10} = 15 \text{ m s}^{-1}$: (a) HH-polarization, (c) VV-polarization. (b), (d) Comparison of geometric optics/two-scale model calculations for $k/k_d = 3$ and the second (SSA-2) small-slope approximation at wind speed $U_{10} = 15 \text{ m s}^{-1}$: (b) HH-polarization, (d) VV-polarization. (e), (f) Comparison of the first (SSA-1) and the second (SSA-2) small-slope approximations for HH- and VV-polarizations: (e) $U_{10} = 5 \text{ m s}^{-1}$, (f) $U_{10} = 15 \text{ m s}^{-1}$.

We do not use such a non-Gaussian assumption, however, the SSA automatically corrects the geometric optics/two-scale model in both the nadir and transitional ranges of incident angles. Figures 1(b) and (d) show a comparison between the geometric optics/two-scale model calculations for $k/k_d = 3$ and the SSA-2 at wind speed $U_{10} = 15 \text{ m s}^{-1}$. The choice of $k/k_d = 3$ looks more reasonable, supporting the conclusion made in [18]. The SSA results appear to be very close to each asymptotic curve at both small and large incidence angles. One can also see in figures 1(b) and (d) that for incidence angles between 20° and 30° , where neither the geometric optics nor the two-scale model is applicable, the SSA provides a smooth transition from the geometric-optics regime to the Bragg scattering regime.

Now we make sure that the calculation of scattering according to the SSA is accurate. A comparison between the SSA-1 and the SSA-2 for HH- and VV-polarizations is shown in figures 1(e) ($U_{10} = 5 \text{ m s}^{-1}$) and (f) ($U_{10} = 15 \text{ m s}^{-1}$). They demonstrate the dependence of the backscattering cross section in the upwind direction for HH- and VV-polarization, σ_{HH} and σ_{VV} , for the K_u -band, as a function of the incidence angle. One can see that the difference between the SSA-1 and SSA-2 for HH-polarization at large incidence angles is less than 2 dB, which could be considered as sufficiently small. This correction is even smaller for VV-polarization. With increasing wind speed, the absolute value of cross sections calculated in the SSA-1 and SSA-2 increases, but the difference between them for VV-polarization is almost constant. For the HH-polarization, the difference between the SSA-1 and SSA-2 increases, but remains within about 2 dB, as is seen from figure 1(f).

To quantify the difference between theoretical and experimental results we use average and maximum mismatches, defined as

$$\langle \delta \rangle = \frac{1}{N_\theta} \sum_{\{\theta\}} |\sigma^{(SSA)}(\theta, \varphi) - \sigma^{(E)}(\theta, \varphi)| \quad (14)$$

and

$$\max \delta = \max_{\{\theta\}} |\sigma^{(SSA)}(\theta, \varphi) - \sigma^{(E)}(\theta, \varphi)| \quad (15)$$

where N_θ is the total number of incidence angles in the set $\{\theta\}$. Scattering cross sections $\sigma^{(SSA)}$ and $\sigma^{(E)}$ in equations (14) and (15) are calculated in dB. The choice of a set of incidence angles $\{\theta\}$ is determined by the empirical models and depends on the wave band. For the K_u -band (SASS-II model) we have $\{\theta\} = 2^\circ, 4^\circ, \dots, 60^\circ$, and for the C-band (CMOD2-I3 model) we have $\{\theta\} = 18^\circ, 19^\circ, \dots, 58^\circ$.

Figure 2 shows the results of calculations of σ_{VV} and σ_{HH} according to the SSA-2 for the K_u -band for wind speeds $U = 5, 10$ and 15 m s^{-1} in upwind ($\varphi = 0$) and downwind ($\varphi = 180^\circ$) directions. For Gaussian statistics of roughness, backscattering in opposite directions is the same, and theoretical curves calculated according to the SSA for upwind and downwind coincide. The experimental results calculated according to the SASS-II model are also shown on the plots.

The errors are demonstrated in table 1. Note that all tables include columns marked ‘no s/w’ corresponding to the contribution from the background spectrum under consideration, and columns marked ‘with s/w’ which include the contribution from steep waves and will be considered in the next section. The rows demonstrating the maximum value of the error $\max \delta$ also include the angle for which this maximum deviation is observed.

One can see that there is good agreement between the theory and the experiment for VV-polarization and for HH-polarization in the downwind direction. However, HH-polarization is severely underestimated for large incidence angles in the upwind direction at all winds. Note that mismatch in absolute values grows with the wind speed, although the level of

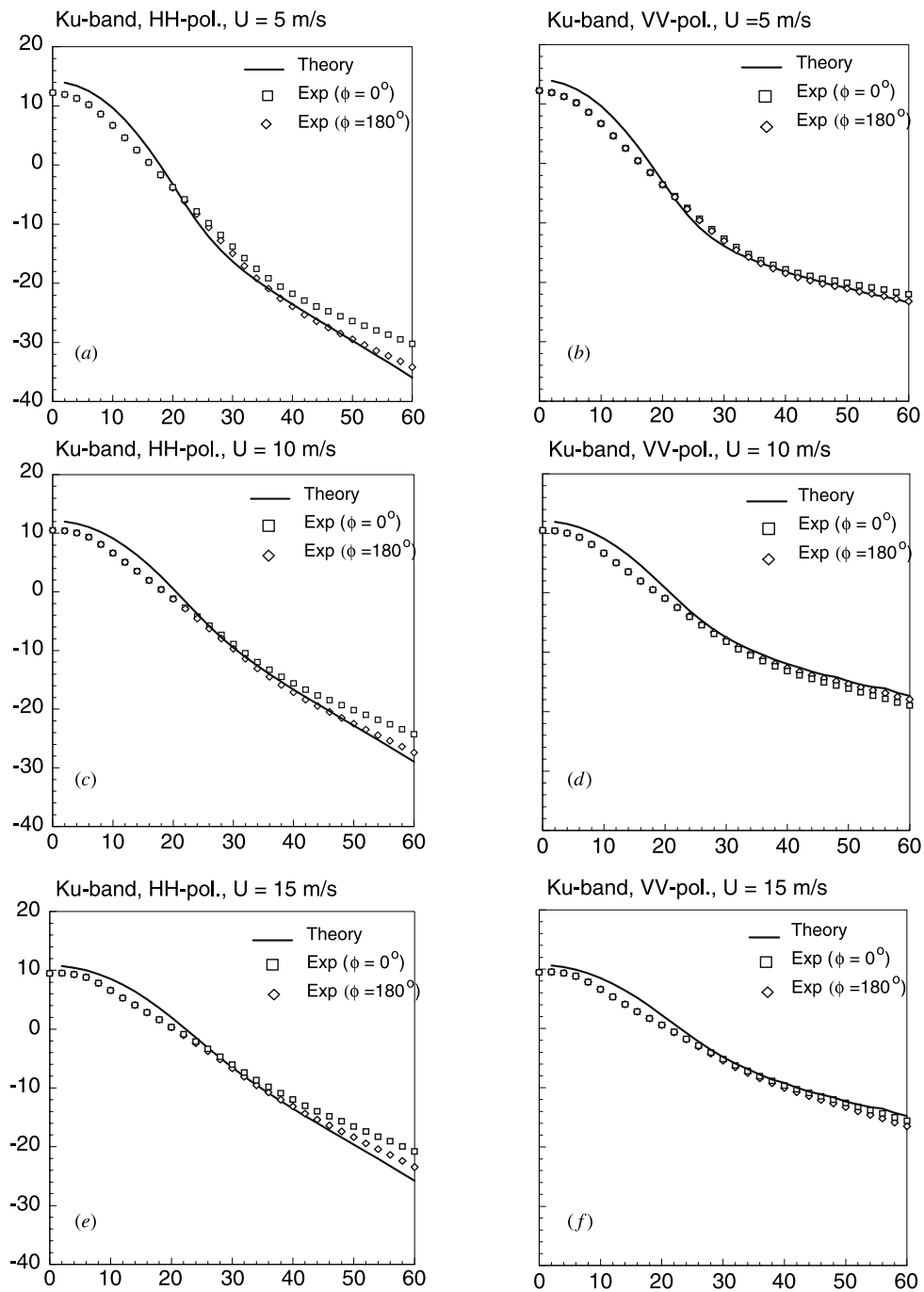


Figure 2. Backscattering cross section for the K_u -band for different wind speeds $U_{10} = 5, 10$ and 15 m s^{-1} in up- ($\phi = 0^\circ$) and downwind ($\phi = 180^\circ$) directions. Both theoretical (SSA-2) and experimental (SASS-II model) results are shown on the plots for both VV- and HH-polarizations.

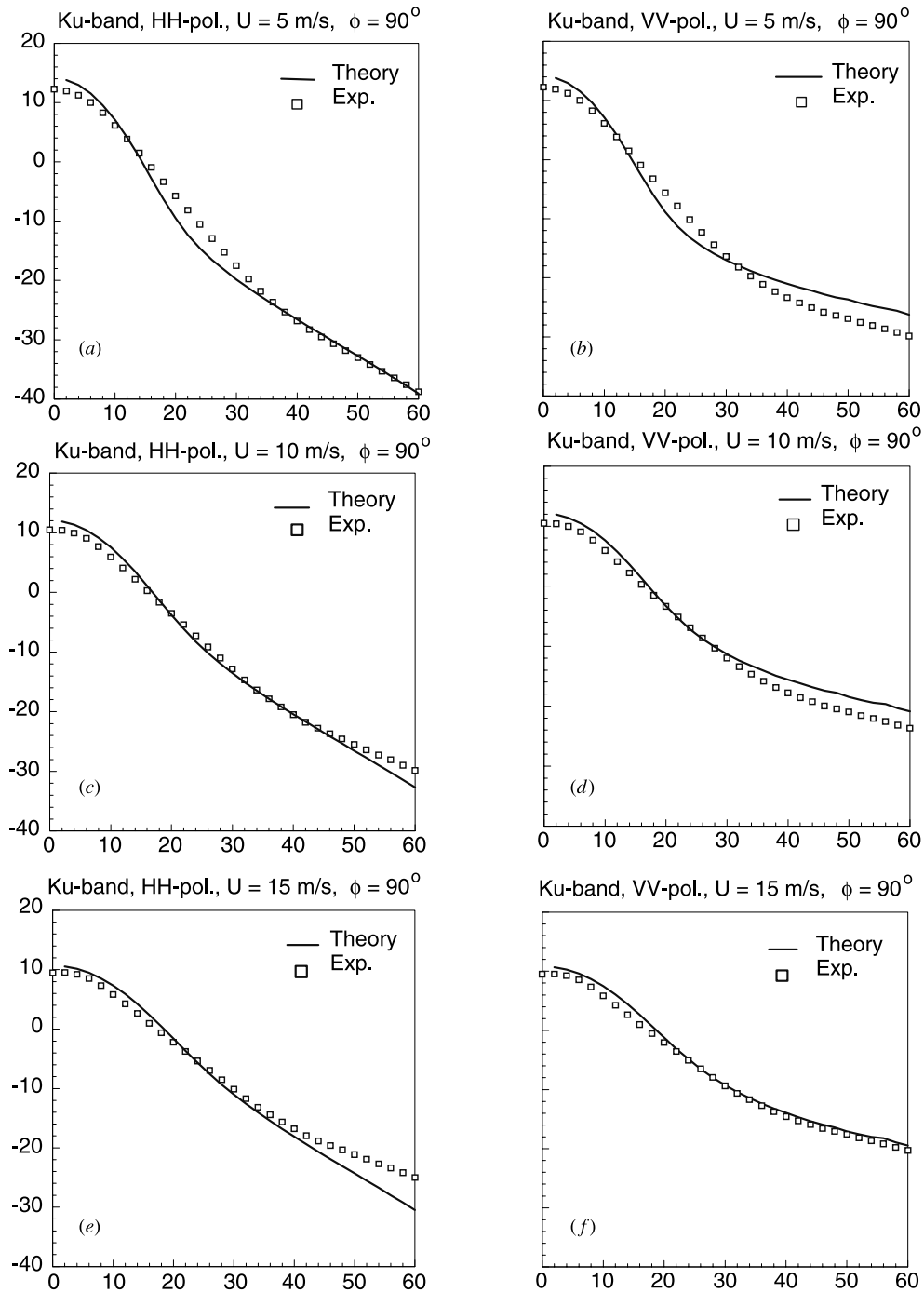


Figure 3. Backscattering cross section for the K_u -band for different wind speeds $U_{10} = 5, 10$ and 15 m s^{-1} in a cross-wind direction ($\phi = 90^\circ$). Both theoretical (SSA-2) and experimental (SASS-II model) results are shown on the plots for both VV- and HH-polarizations.

Table 1. Errors for along-wind directions; K_u -band.

φ	δ (dB)	5 m s^{-1}		10 m s^{-1}		15 m s^{-1}	
		No s/w	With s/w	No s/w	With s/w	No s/w	With s/w
0°	δ_V	1.3	1.0	1.1	1.3	0.9	1.2
180°	δ_V	1.0	1.0	1.5	1.5	1.2	1.2
0°	δ_H	2.6	0.9	1.9	0.9	1.9	0.7
180°	δ_H	1.2	1.2	1.1	1.1	1.2	1.2
0°	max δ_V	3.1	3.1	2.8	2.8	2.3	2.3
	θ	12°	12°	14°	14°	14°	14°
180°	max δ_V	3.1	3.1	2.8	2.8	2.3	2.3
	θ	12°	12°	14°	14°	14°	14°
0°	max δ_H	5.7	3.1	4.7	2.8	5.0	2.3
	θ	60°	12°	60°	14°	60°	14°
180°	max δ_H	3.1	3.1	2.8	2.8	2.3	2.3
	θ	12°	12°	14°	14°	60°	60°

underestimation on a dB scale stays roughly the same. The HH-polarization cross section at K_u -band for the cross-wind direction (see figure 3, left-hand column) is also underestimated at large incidence angles for higher winds, although to a lesser extent than for the upwind direction. At the same time, for a 5 m s^{-1} wind speed the HH-polarization is in good correspondence with the experiment. However, the VV-polarization is somewhat overestimated for 5 and 10 m s^{-1} winds. As in the K_u -band case, the backscattering cross section for the C-band in the cross-wind direction (figure 4, right-hand column) for 5 and 10 m s^{-1} winds is also overestimated. This behaviour seems to be inconsistent with the along-wind cases, where the VV-polarization was accurately predicted in both directions. For this reason, we suspect that the directional part of the Elfouhaily *et al* [34] surface spectrum overestimates the spectral density of short, centimetre-length waves by 2–4 dB in the cross-wind direction, and a modification should be introduced to it. A specific modification of the directional part of the Elfouhaily *et al* [34] surface spectrum was suggested in our paper [44] based on a comparison between experimental and calculated second-order azimuthal harmonics of the K_u - and C-band radar cross sections. This modification would reduce calculated backscattering at both polarizations, thus bringing the VV-polarization in line with experiment. As a result, the HH-polarization would be underestimated, similar to the upwind case. We do not use the modification here since a major focus in this paper is on the along-wind behaviour of the radar cross section, but the interested reader can refer to our paper [44].

For the C-band the results for the VV-polarization are shown in figure 4 (left-hand column), and corresponding errors are demonstrated in table 2 (the CMOD2-I3 model is not available for HH-polarization). There is good correspondence between theory and experiment, especially for higher winds. For a 5 m s^{-1} wind speed, the backscattering cross section is underestimated by 2–3 dB for moderate incidence angles between 20° and 43° .

Both the sea-roughness spectrum and the empirical models of scattering represent the results of averaging over broad ensembles of environmental situations corresponding to a given wind. Those ensembles include cases that differ in many respects such as wave age (in our simulations we assumed a fully developed sea), history of wave and wind field, atmospheric stability, and others. The non-uniformity of environmental conditions over a single resolution cell could play a negative role in wind retrieval and interpretation of satellite scatterometric data. The problem of wind variability on scatterometry at low wind speeds is addressed by

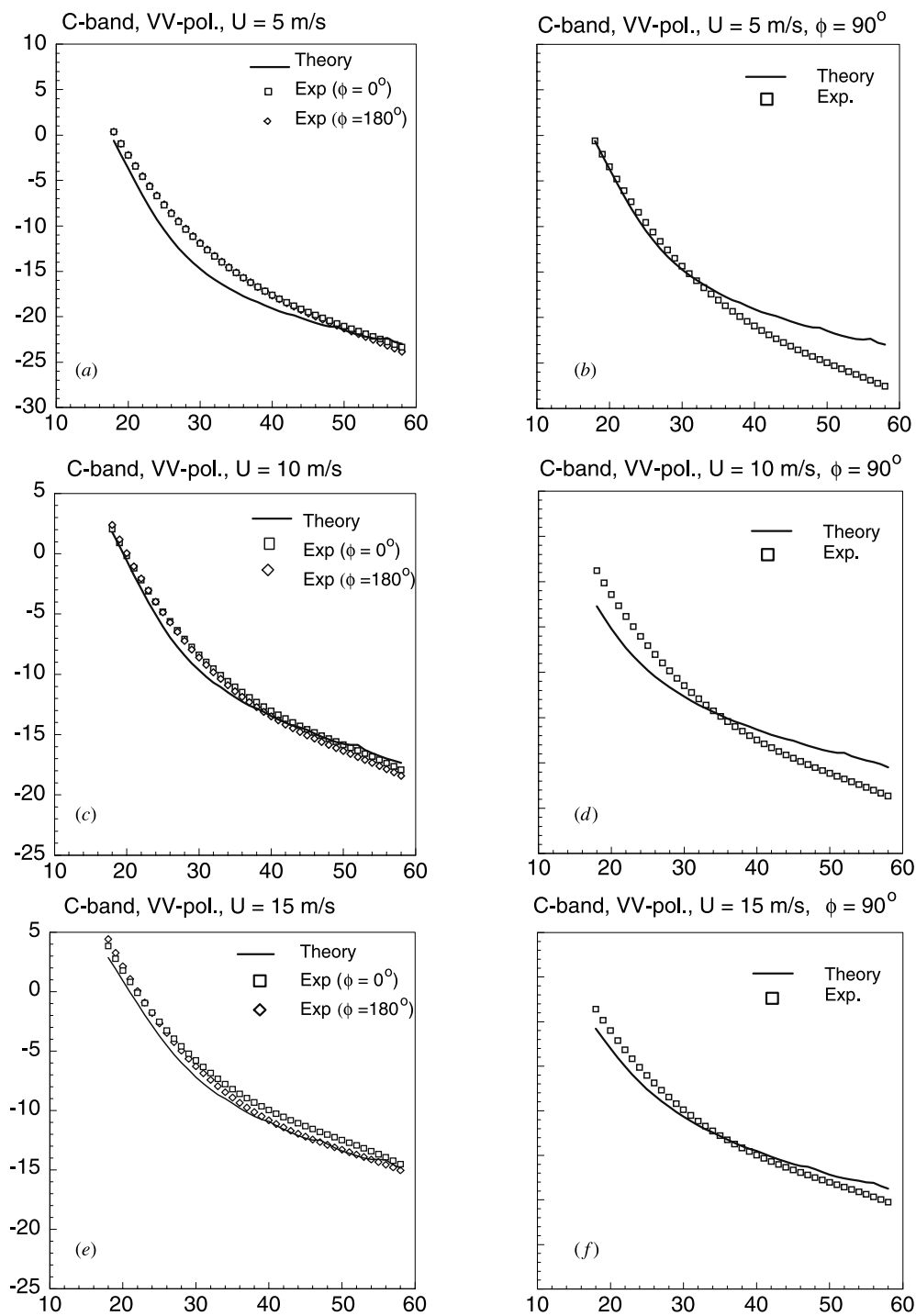


Figure 4. Backscattering cross section for the C-band for different wind speeds $U_{10} = 5, 10$ and 15 m s^{-1} in upwind ($\phi = 0^\circ$) and downwind ($\phi = 180^\circ$) directions ((a), (c) and (e)), and in the cross-wind direction ($\phi = 90^\circ$) ((b), (d) and (f)). Experimental data are calculated according to the CMOD2-I3 model (there is no model for the HH-polarization for the C-band).

Table 2. Errors for along-wind directions; C-band.

φ	δ (dB)	5 m s^{-1}		10 m s^{-1}		15 m s^{-1}	
		No s/w	With s/w	No s/w	With s/w	No s/w	With s/w
0°	δ_V	1.5	2.8	0.6	0.6	1.0	0.6
180°	δ_V	1.5	1.5	0.8	0.7	0.5	0.5
0°	$\max \delta_V$	2.9	4.2	1.4	1.4	1.4	1.4
	θ	28°	56°	27°	27°	30°	30°
180°	$\max \delta_V$	3.0	3.0	1.2	1.2	1.6	1.6
	θ	28°	28°	27°	27°	18°	18°

Plant [13]. Indeed, the backscattering cross section σ is a nonlinear functional of the roughness spectrum S , and generally

$$\langle \sigma(S) \rangle \neq \{ \sigma \langle S \rangle \} \quad (16)$$

where $\langle \cdot \rangle$ denotes averaging over different environmental conditions with a given wind. With consideration of this fact, and remembering that the Elfouhaily *et al* spectrum was developed without any reference to remote sensing data [34] and that our scattering model has not used any adjustment parameters, the overall correspondence between theoretical calculations and experimental data should be considered as good.

However, correspondence between theory and experiment cannot be considered satisfactory for the HH-polarization at large incidence angles in the upwind direction. The difference between the second and the first order of the SSA does not exceed 2.7 dB in this case (see figure 1(f), the 15 m s^{-1} wind-speed case). Therefore, the underestimate of σ_{HH} by 5–6 dB seen in figures 2(a)–(c) for all three wind speeds cannot be attributed to the inaccuracy of scattering calculations. Moreover, theoretical results describe scattering in the downwind direction very well. Thus, we conclude that in contrast to the downwind case, the model of sea roughness is not quite adequate with respect to scattering in the upwind direction.

The difference between upwind and downwind backscattering is described by the first azimuthal harmonic of the backscattering cross section. The polarization ratio corresponding to this harmonic according to the SASS-II empirical model at large incident angles differs from that predicted by the two-scale model. This suggests an additional mechanism of backscattering which is considered in the next section.

4. The effect of steep waves

In this section we will correct the problem of underestimation of HH-polarization results for large incidence angles in the upwind and cross-wind directions by invoking contributions from steep, breaking waves. Their potential importance for polarization behaviour of microwave backscattering has been acknowledged by many authors (see, e.g., [46–52]).

Let us assume that apart from a background of relatively smooth waves represented by the Elfouhaily *et al* [34] spectrum, the rough sea surface includes a small percentage of steep waves with slope angles in the range of 30° – 60° . Such waves provide a contribution to the backscattering cross section by specularly reflecting back a small part of the incident power. We assume here for simplicity that this process can be described in the geometric optics approximation. Since the percentage of the sea surface covered by such steep waves is

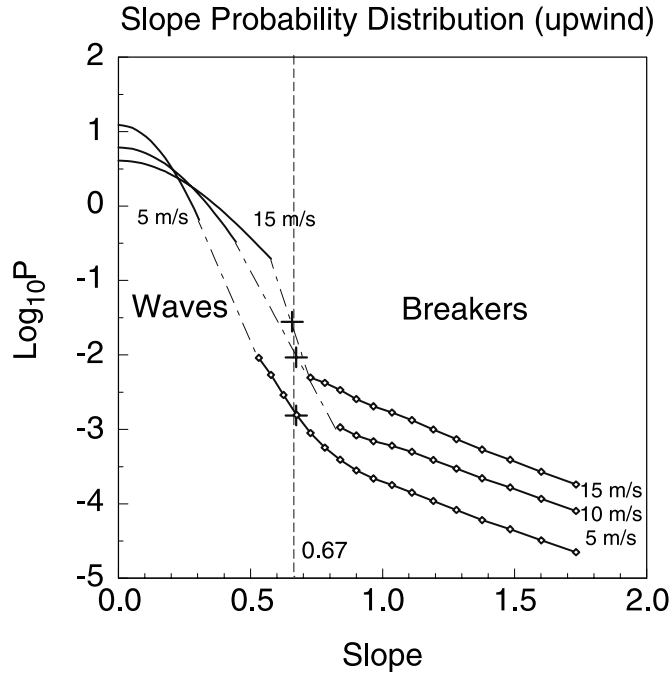


Figure 5. Probability distribution of slopes P (on a logarithmic scale) for the upwind direction for three wind speeds. At small slopes P is calculated according to the Cox–Munk results [35, 36]. Crosses demonstrate whitecapping coverage calculated according to [54].

small, we can simply add it to the backscattering cross section previously calculated according to the SSA:

$$\sigma(\theta, \varphi) = \sigma^{(SSA)}(\theta, \varphi) + \pi \frac{|V_0|^2}{\cos^4 \theta} P \quad (17)$$

where $V_0 = (\sqrt{\varepsilon} - 1)/(\sqrt{\varepsilon} + 1)$ is the Fresnel reflection coefficient at normal incidence. Note that the function P in equation (17) is a probability density function $P(\vec{a})$ of slopes $\vec{a} = \nabla h$, where h is the elevation of steep waves. The slope is related to polar angles of the normal to the facet through the following relation:

$$a_x = -\tan \theta \cos \varphi \quad a_y = -\tan \theta \sin \varphi. \quad (18)$$

The probability density function of steep slopes P cannot be calculated from a Cox–Munk distribution since such slopes are beyond the limits of its validity [35, 36, 52]. We determined P from equation (17) by substituting for σ experimental values for the HH-polarization measured in the K_u -band. The function P was calculated for slope angles θ exceeding 30° , and only when the difference between experimental and calculated values at the HH-polarization exceeded 1 dB. The results for the upwind direction ($a_y = \varphi = 0$) are shown in figure 5 for three wind speeds. They are arbitrarily interpolated to the Cox–Munk distribution within the validity limits of the latter. The area of negative slopes (the downwind direction) for P is not shown in figure 5, but in our consideration it is simply the Cox–Munk distribution symmetrically extended into the area of negative slopes. Therefore, the resulting probability distribution function P represents a non-Gaussian, skewed distribution. For more details on scattering from non-Gaussian surfaces the interested reader can refer to [53].

One can see that P for steep waves increases with the wind and decreases with slope angle θ . Three crosses on the same plot mark values $W_U = 2.2 \times 10^{-5} U^{2.71}$ that represent an estimate of the part of the sea surface covered by whitecaps [54] (wind speed U is measured in m s^{-1} in this formula). The waves with slopes roughly exceeding 30° (corresponding to surface gravity waves with a critical angle at the crest of 120°) cannot be stable, and while overturning they generate breakers with even steeper slopes for a short period of time. As a result of wave breaking, whitecaps are formed on the sea surface. It is interesting to note that W_U corresponds to the same slope of 34° at all winds. This angle is close to the limiting slope. Thus, calculated values of the probability density function P of large surface slopes based on radar scatterometric data are consistent with the anticipated properties of the wave breaking. The function P at $a_y = 0$ can be approximated by the following simple formula:

$$\log_{10} P(a_x, 0) = -2.84 + 0.097U - 1.33a_x \quad (19)$$

where U is a wind speed in m s^{-1} (at 10 m height) and $a_x > 0.8$ (strictly speaking, a_x in equation (19) should be negative since waves overturn in the direction of the wind, but for simplicity here we changed the sign of a_x to positive).

The probability of slopes in the cross-wind direction that were calculated in a similar way are demonstrated in figure 6. Corresponding probabilities are smaller than in the upwind direction, which is expected. We have not analysed P in this case in detail because we question the accuracy of the Elfouhaily *et al* [34] spectrum in the cross-wind direction.

In figures 7 and 8 the backscattering cross sections are calculated, taking into account the contribution from steep waves in the upwind and cross-wind directions. (There is no need to introduce steep-wave corrections for the downwind direction.) A perfect agreement with respect to the HH-polarization in figure 7 is ensured by the way we have calculated the function P . One can see that the results with respect to the VV-polarization have almost not changed and the agreement remains good, since the contribution to backscattering from steep waves is much smaller than that to scattering from the background waves for VV-polarization. It is interesting to note that for the C-band at 5 m s^{-1} wind speed, the contribution from steep waves resulted in a significant improvement of VV-polarization return for incidence angles between 30° and 40° . For 15 m s^{-1} in the C-band we obtained a perfect fit with experimental data in the upwind direction for all angles greater than 35° . Visible kinks on curves are results of using correcting contributions from breaking waves only for slope angles θ exceeding 30° , and only when the difference between experimental and calculated values at the HH-polarization exceeded 1 dB.

Table 3. Errors for cross-wind direction; both bands.

Band	δ (dB)	5 m s^{-1}		10 m s^{-1}		15 m s^{-1}	
		No s/w	With s/w	No s/w	With s/w	No s/w	With s/w
K_u	δ_V	2.2	2.2	1.6	1.7	0.8	1.1
K_u	δ_H	1.3	1.1	1.0	0.6	1.8	0.5
C	δ_V	2.4	3.7	2.1	2.1	1.0	1.4
K_u	max δ_V	3.7	3.7	2.9	3.2	1.8	1.8
	θ	58°	58°	56°	56°	14°	14°
K_u	max δ_H	4.1	4.1	2.8	1.6	5.4	1.6
	θ	22°	22°	60°	10°	60°	12°
C	max δ_V	5.8	5.8	3.9	3.9	2.2	2.4
	θ	18°	18°	18°	18°	18°	56°

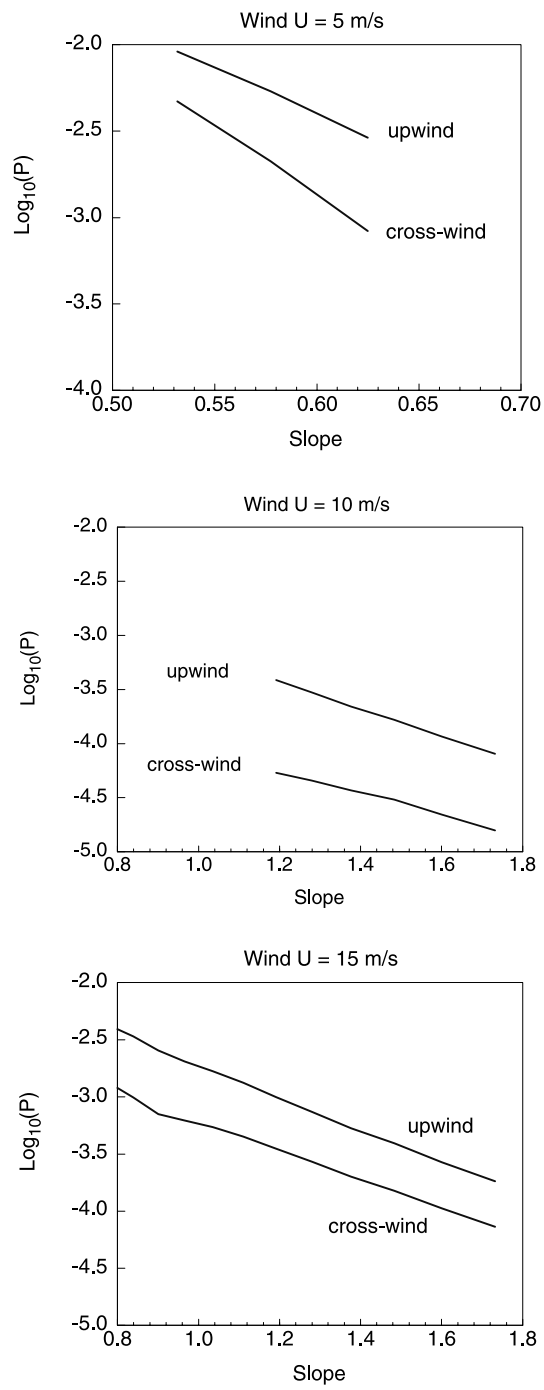


Figure 6. Comparisons between upwind and cross-wind values of the probability distribution function P (on a logarithmic scale) for three wind speeds.

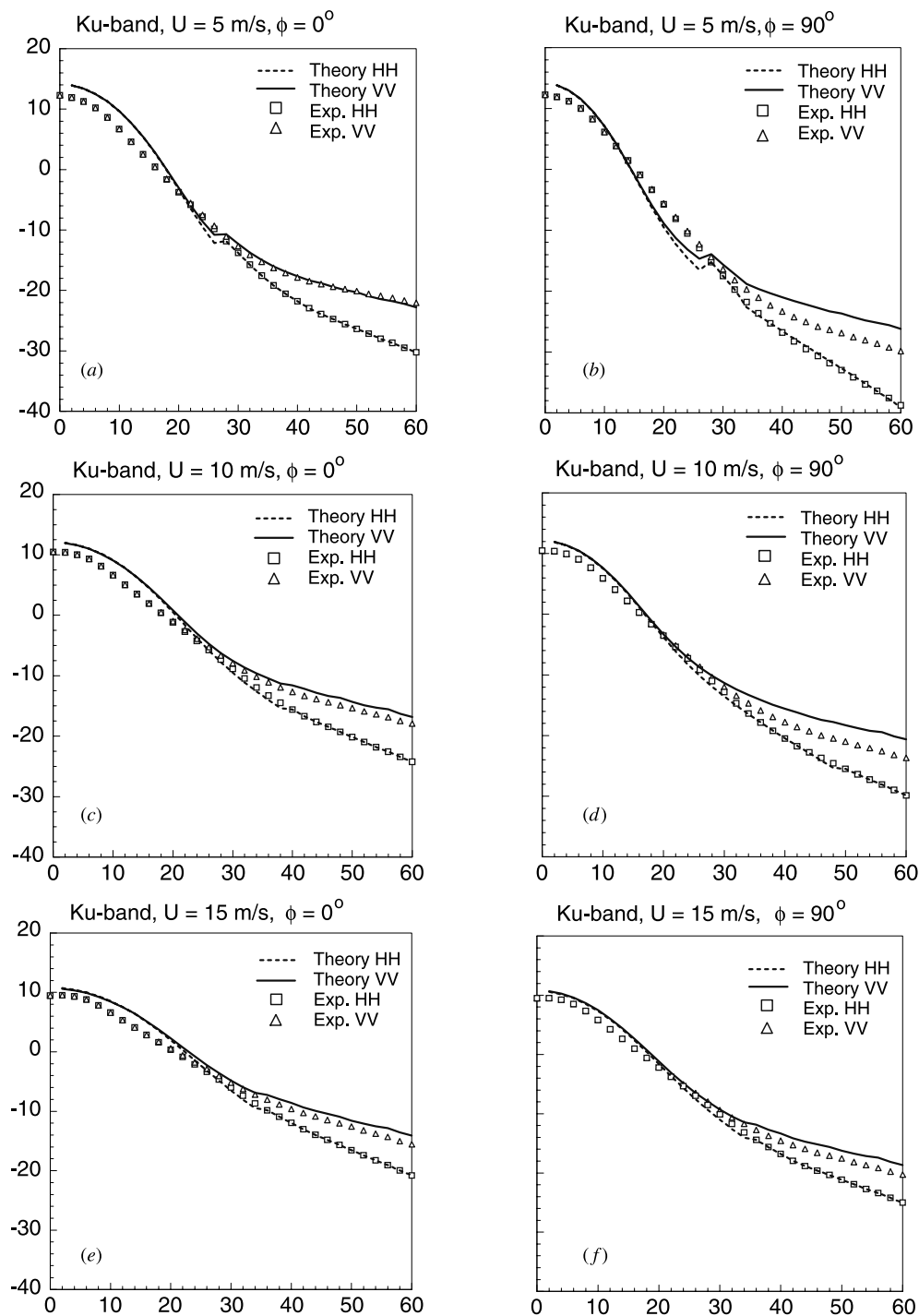


Figure 7. Backscattering cross sections for three wind speeds in the upwind and cross-wind directions for the K_u -band with the effect of steep waves included. Perfect correspondence between theory and experiment for the HH-polarization case is ensured by the way we calculated the probability distribution function P .

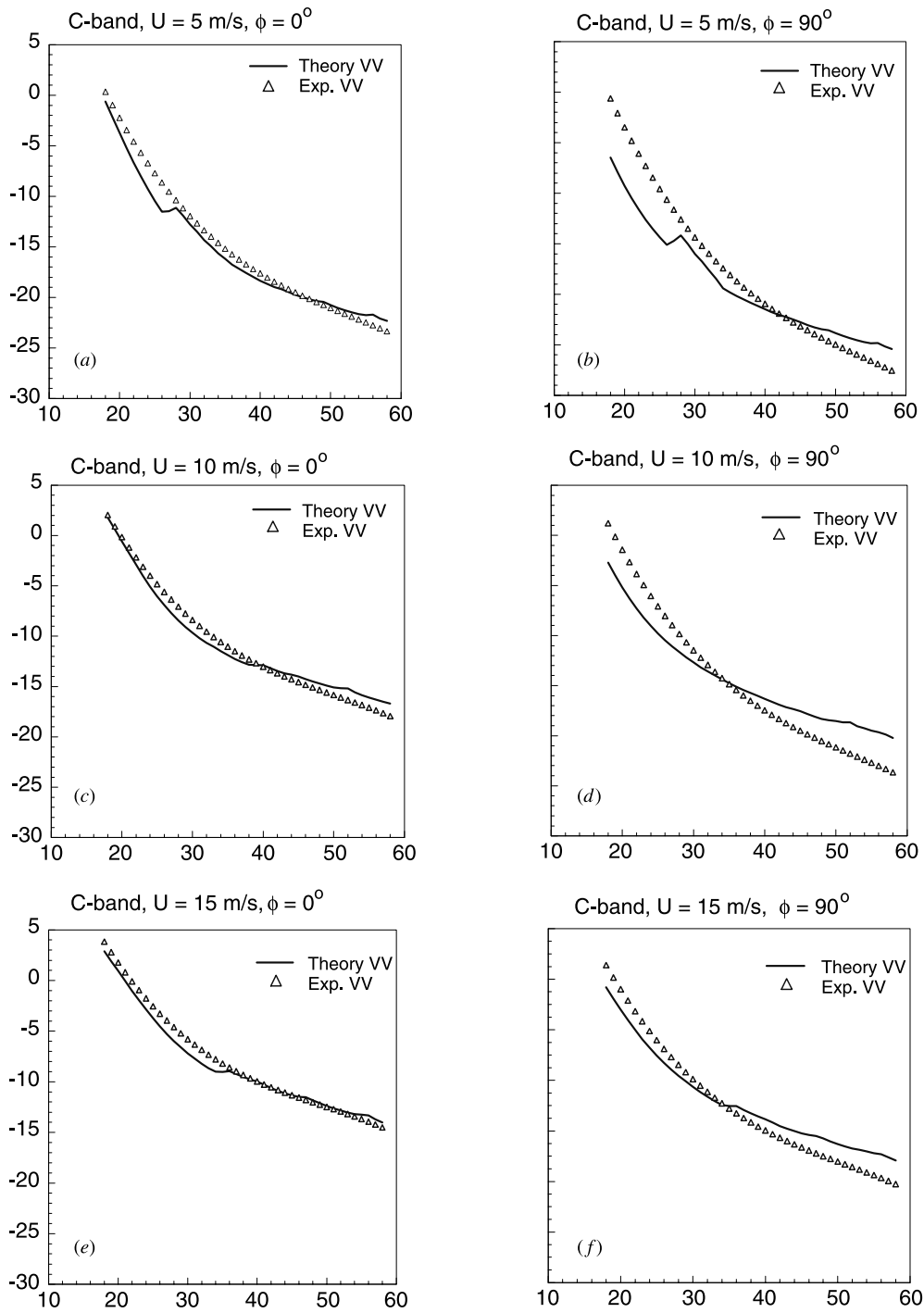


Figure 8. Backscattering cross sections for three wind speeds in the upwind and cross-wind directions for the C-band with the effect of steep waves included.

Appropriate errors are also demonstrated in columns of tables 1–3 marked ‘with s/w ’. One can see that in most cases a maximum error of the order of 3 dB is observed now at moderate incidence angles of $\theta = 12^\circ$ – 14° for the K_u -band and $\theta = 28^\circ$ – 32° for the C-band. The error tends to be greater for low winds. The reason for this discrepancy is not clear. It could be related to the larger variability in the long-wave component of the spectrum which is more affected by factors other than local wind, or due to the effect of wind variability over the resolution cell discussed in [13]. As a result the difference between the right- and left-hand sides of equation (16) becomes more pronounced for smaller incidence angles where the Kirchhoff mechanism significantly contributes to backscattering.

5. Conclusions

We have calculated the backscattering cross section as a function of incidence angle in the upwind, downwind and cross-wind directions for K_u - and C-bands for three wind speeds of 5, 10 and 15 m s^{-1} and compared the results with averaged experimental data provided by the empirical models SASS-II and CMOD2-I3. Calculations were performed with the help of the small-slope approximation, which allows control of the accuracy of scattering calculations. Sea roughness was assumed to obey Gaussian statistics and the Elfouhaily *et al* [34] spectrum of roughness was used in numerical calculations. The results of calculations appeared to be in good overall agreement with empirical models with the exception of the HH-polarization in the upwind (and to a lesser extent in the cross-wind) direction. This discrepancy in the along-wind direction was attributed to contributions from steep slopes of breakers (see figure 5). This hypothesis allowed us to calculate the probability distribution function P of steep breaking waves which appeared to be reasonable. A simple approximate formula for P given by equation (19) was suggested for the case of the upwind direction. Calculation of backscattering taking into account steep breaking waves (the geometric optics approximation was assumed to be valid) provided results that coincide with empirical models within 1–2 dB accuracy for all winds, incidence, and azimuthal angles and polarizations.

The lowest accuracy was observed in the cross-wind direction both for K_u - and C-bands for 5 and 10 m s^{-1} wind speed. In contrast to the upwind and downwind cases, the VV-polarization is now overestimated for large incidence angles (and the HH-polarization appears to be in good agreement with the experiment). We believe that the reason for this is an overestimation of the appropriate part of the small-scale roughness in the cross-wind direction made by the Elfouhaily *et al* [34] spectrum at relatively low winds. When this part of the small-scale spectrum is reduced by 2–4 dB, the VV-polarization will be close to that of experiment for all azimuthal angles, and backscattering from the background spectrum for the HH-polarization in the cross-wind direction will be underestimated quite similarly to that in the upwind case, but to a lesser extent. Thus, we believe that the Elfouhaily *et al* [34] spectrum at relatively low winds in the cross-wind direction should be modified in the manner suggested in [44]. For this reason we have not analysed in great detail the probability density function of steep slopes in this case.

Of course, the contribution from steep breaking waves is only one possible explanation of the underestimation of HH-polarization at large incidence angles. This explanation was considered in the literature previously, but mainly on a qualitative level. Our investigation provides a quantitative estimate of the parameters of steep waves that follows from this hypothesis. Other explanations consider the effects of hydrodynamic modulation of small-scale waves and their amplification at the front faces of long waves; however, complete agreement with the experiment has not yet been achieved [26]. The ultimate test for the above-considered hypothesis could be provided by experimental measurements of the surface-

slope probability distribution function at large slopes and a comparison with the results given by equation (19).

Note that both experimental and theoretical results show that the data can be accurately approximated by only three azimuthal harmonics (the zeroth, first and second ones). Hence, a good fit between the theory and the experiment in upwind, downwind and cross-wind directions ensures appropriately good results for all azimuthal angles.

A practical implication of this work is its potential as a method to increase the accuracy of wind-speed retrieval from scatterometric measurements similar to the two-scale-model algorithm proposed in [25], but instead based on the above-discussed theoretical approach. The long-wave component of the wave field can be calculated by taking into account all the pertinent factors by using the appropriate WAM-type wave-prediction model [55]. Then the short-wave component can be estimated based on the values of local wind, and matched to the results of the calculation of the backscattering cross section for different winds.

Acknowledgment

The authors would like to thank E Walsh of the NASA Goddard Space Flight Center, Greenbelt, MD, USA, for discussions and helpful suggestions.

Appendix

The general expressions for kernel functions B and B_2 on the basis of vertically and horizontally polarized waves are given in [32] and are as follows. The first order:

$$B_{11}(\vec{k}, \vec{k}_0) = \frac{\varepsilon - 1}{(\varepsilon q_k^{(1)} + q_k^{(2)})(\varepsilon q_0^{(1)} + q_0^{(2)})} \left(q_k^{(2)} q_0^{(2)} \frac{\vec{k} \vec{k}_0}{kk_0} - \varepsilon k k_0 \right) \quad (\text{A1})$$

$$B_{12}(\vec{k}, \vec{k}_0) = \frac{\varepsilon - 1}{(\varepsilon q_k^{(1)} + q_k^{(2)})(q_0^{(1)} + q_0^{(2)})} \frac{\omega}{c} q_k^{(2)} \frac{\vec{N}[\vec{k}, \vec{k}_0]}{kk_0} \quad (\text{A2})$$

$$B_{21}(\vec{k}, \vec{k}_0) = \frac{\varepsilon - 1}{(q_k^{(1)} + q_k^{(2)})(\varepsilon q_0^{(1)} + q_0^{(2)})} \frac{\omega}{c} q_0^{(2)} \frac{\vec{N}[\vec{k}, \vec{k}_0]}{kk_0} \quad (\text{A3})$$

$$B_{22}(\vec{k}, \vec{k}_0) = - \frac{\varepsilon - 1}{(q_k^{(1)} + q_k^{(2)})(q_0^{(1)} + q_0^{(2)})} \frac{\omega^2}{c^2} \frac{\vec{k} \vec{k}_0}{kk_0}. \quad (\text{A4})$$

The second order:

$$\begin{aligned} (B_2)_{11}(\vec{k}, \vec{k}_0; \vec{\xi}) &= \frac{\varepsilon - 1}{(\varepsilon q_k^{(1)} + q_k^{(2)})(\varepsilon q_0^{(1)} + q_0^{(2)})} \left[-2 \frac{\varepsilon - 1}{\varepsilon q_\xi^{(1)} + q_\xi^{(2)}} \left(q_k^{(2)} q_0^{(2)} \frac{\vec{k} \vec{\xi}}{k} \frac{\vec{\xi} \vec{k}_0}{k_0} + \varepsilon k k_0 \xi^2 \right) \right. \\ &+ 2\varepsilon \frac{q_\xi^{(1)} + q_\xi^{(2)}}{\varepsilon q_\xi^{(1)} + q_\xi^{(2)}} \left(k_0 q_k^{(2)} \frac{\vec{k} \vec{\xi}}{k} + k q_0^{(2)} \frac{\vec{\xi} \vec{k}_0}{k_0} \right) \\ &\left. - \left(\varepsilon \frac{\omega^2}{c^2} (q_k^{(2)} + q_0^{(2)}) + 2q_k^{(2)} q_0^{(2)} (q_\xi^{(1)} - q_\xi^{(2)}) \right) \frac{\vec{k} \vec{k}_0}{kk_0} \right] \quad (\text{A5}) \end{aligned}$$

$$\begin{aligned}
(B_2)_{12}(\vec{k}, \vec{k}_0; \vec{\xi}) &= \frac{(\varepsilon - 1)\omega/c}{(\varepsilon q_k^{(1)} + q_k^{(2)})(q_0^{(1)} + q_0^{(2)})} \left[-2 \frac{\varepsilon - 1}{\varepsilon q_\xi^{(1)} + q_\xi^{(2)}} q_k^{(2)} \frac{\vec{k}\vec{\xi}}{k} \frac{\vec{N}[\vec{\xi}, \vec{k}_0]}{k_0} \right. \\
&\quad + 2\varepsilon \frac{q_\xi^{(1)} + q_\xi^{(2)}}{\varepsilon q_\xi^{(1)} + q_\xi^{(2)}} k \frac{\vec{N}[\vec{\xi}, \vec{k}_0]}{k_0} \\
&\quad \left. - \left(\varepsilon \frac{\omega^2}{c^2} + q_k^{(2)} q_0^{(2)} + 2q_k^{(2)}(q_\xi^{(1)} - q_\xi^{(2)}) \right) \frac{\vec{N}[\vec{k}, \vec{k}_0]}{kk_0} \right] \quad (A6)
\end{aligned}$$

$$\begin{aligned}
(B_2)_{21}(\vec{k}, \vec{k}_0; \vec{\xi}) &= \frac{(\varepsilon - 1)\omega/c}{(q_k^{(1)} + q_k^{(2)})(\varepsilon q_0^{(1)} + q_0^{(2)})} \left[2 \frac{\varepsilon - 1}{\varepsilon q_\xi^{(1)} + q_\xi^{(2)}} q_0^{(2)} \frac{\vec{k}_0\vec{\xi}}{k_0} \frac{\vec{N}[\vec{\xi}, \vec{k}]}{k} \right. \\
&\quad - 2\varepsilon \frac{q_\xi^{(1)} + q_\xi^{(2)}}{\varepsilon q_\xi^{(1)} + q_\xi^{(2)}} k_0 \frac{\vec{N}[\vec{\xi}, \vec{k}]}{k} \\
&\quad \left. - \left(\varepsilon \frac{\omega^2}{c^2} + q_k^{(2)} q_0^{(2)} + 2q_0^{(2)}(q_\xi^{(1)} - q_\xi^{(2)}) \right) \frac{\vec{N}[\vec{k}, \vec{k}_0]}{kk_0} \right] \quad (A7)
\end{aligned}$$

$$\begin{aligned}
(B_2)_{22}(\vec{k}, \vec{k}_0; \vec{\xi}) &= \frac{\varepsilon - 1}{(q_k^{(1)} + q_k^{(2)})(q_0^{(1)} + q_0^{(2)})} \frac{\omega^2}{c^2} \left[-2 \frac{\varepsilon - 1}{\varepsilon q_\xi^{(1)} + q_\xi^{(2)}} \left(\frac{\vec{k}\vec{\xi}}{k} \frac{\vec{\xi}\vec{k}_0}{k_0} - \xi^2 \frac{\vec{k}\vec{k}_0}{kk_0} \right) \right. \\
&\quad \left. + (q_k^{(2)} + q_0^{(2)} + 2(q_\xi^{(1)} - q_\xi^{(2)})) \frac{\vec{k}\vec{k}_0}{kk_0} \right]. \quad (A8)
\end{aligned}$$

Here $q_k^{(1,2)}$ and $-q_0^{(1,2)}$ are the vertical components of the appropriate wavevectors in the first (air) and the second (dielectric) medium:

$$q_k^{(1)} = \sqrt{\frac{\omega^2}{c^2} - k^2} \quad q_k^{(2)} = \sqrt{\varepsilon \frac{\omega^2}{c^2} - k^2} \quad \text{Im } q_k^{(1,2)} \geq 0 \quad (A9)$$

$$q_0^{(1)} = \sqrt{\frac{\omega^2}{c^2} - k_0^2} \quad q_0^{(2)} = \sqrt{\varepsilon \frac{\omega^2}{c^2} - k_0^2} \quad \text{Im } q_0^{(1,2)} \geq 0 \quad (A10)$$

(ε is a generally complex dielectric constant). Note that in section 2 we use a simplified notation: $q_k \equiv q_k^{(1)}$ and $q_0 \equiv q_0^{(1)}$. The vector $\vec{N} = (0, 0, 1)$ above is a unit normal to the horizontal plane.

References

- [1] Jones W L, Schroeder L C and Mitchell J L 1977 Aircraft measurements of the microwave scattering signature of the ocean *IEEE J. Ocean Eng.* **2** 52–61
- [2] Jones W L, Schroeder L C, Boggs D H, Bracalente E M, Brown R A, Dome G J, Pierson W J and Wentz F J 1982 The SEASAT-A satellite scatterometer: the geophysical evaluation of remotely sensed wind vectors over the ocean *J. Geophys. Res.* **87** 3297–317
- [3] Wentz F J, Peteherich S and Thomas L A 1984 A model function for ocean radar cross-section at 14.6 GHz *J. Geophys. Res.* **89** 3689–704
- [4] Attema E W 1991 The active microwave instrument on-board the ERS-1 satellite *Proc. IEEE* **79** 791–9
- [5] Stoffelen A and Anderson D L T 1993 ERS-1 scatterometer data and characteristics and wind retrieval skills *Proc. 1st ERS-1 Symp.* European Space Agency, SP-359
- [6] Offiler D 1994 The calibration of ERS-1 satellite scatterometer winds *J. Atmos. Ocean. Technol.* **11** 1002–17
- [7] Bentamy A, Queffeuilou P, Quilfen Y and Katsaros K 1999 Ocean surface wind fields estimated from satellite active and passive microwave instruments *IEEE Trans. Geosci. Remote Sens.* **37** 2469–86

- [8] Wentz F J 1999 A model function for the ocean-normalized radar cross section at 14 GHz derived from NSCAT observations *J. Geophys. Res.* **104** 11 499–514
- [9] Liu Y and Pierson W J 1994 Comparisons of scatterometric models for the AMI on ERS-1: the possibility of systematic azimuth angle biases of wind speed and direction *IEEE Trans. Geosci. Remote Sens.* **32** 626–35
- [10] Nghiem S V, Li F K and Neumann G 1997 The dependence of ocean backscatter at Ku-band on oceanic and atmospheric parameters *IEEE Trans. Geosci. Remote Sens.* **35** 581–600
- [11] Quilfen Y, Chapron B, Elfouhaily T, Katsaros K and Tournadre J 1998 Observation of tropical cyclones by high-resolution scatterometry *J. Geophys. Res.* **103** 7767–86
- [12] Austin S and Pierson W J 1999 mesoscale and synoptic-scale effects on the validation of NSCAT winds by means of data buoy reports *J. Geophys. Res.* **104** 11 437–47
- [13] Plant W J 2000 Effects of wind variability on scatterometry at low wind speeds *J. Geophys. Res.* **105** 16 899–910
- [14] Carswell J R, Carson S C, McIntosh R E, Li F K, Neumann G, McLaughlin D J, Wilkerson J C, Black P G and Nghiem S V 1994 Airborne scatterometers: investigating ocean backscatter under low- and high-wind conditions *Proc. IEEE* **82** 1835–60
- [15] Donnelly W J, Carswell J R, McIntosh R E, Chang P S, Wilkerson J, Marks F and Black P G 1999 Revised ocean backscatter model at C and Ku band under high-wind conditions *J. Geophys. Res.* **104** 11 485–97
- [16] Chan H L and Fung A K 1977 A theory of sea scatter at large incidence angles *J. Geophys. Res.* **82** 3439–44
- [17] Wentz F J 1977 A two-scale scattering model with application to the JONSWAP 75 aircraft microwave scatterometer experiment *NASA Contract Rep. 2919* (December)
- [18] Brown G S 1978 Backscattering from a Gaussian-distributed, perfectly conducting rough surface *IEEE Trans. Antennas Propagat.* **26** 472–82
- [19] Brown G S 1979 Estimation of surface wind speeds using satellite-borne measurements at normal incidence *J. Geophys. Res.* **84** 3974–8
- [20] Fung A K and Lee K K 1982 A semi-empirical sea-spectrum model for scattering coefficient estimation *IEEE J. Ocean. Eng.* **7** 166–76
- [21] Durden S L and Vesecky J F 1985 A physical radar cross-section model for a wind-driven sea with swell *IEEE J. Ocean. Eng.* **10** 445–51
- [22] Plant W J 1986 Two-scale model for short wind-generated waves and scatterometry *J. Geophys. Res.* **91** 10 735–49
- [23] Donelan M A and Pierson W J 1987 Radar scattering and equilibrium ranges in wind-generated waves with application to scatterometry *J. Geophys. Res.* **92** 4971–5029
- [24] Thompson D R 1988 Calculation of radar backscatter modulations from internal waves *J. Geophys. Res.* **93** 12 371–80
- [25] Janssen P A E M, Wallbrink H, Calkoen C J, van Halsema D, Oost W A and Snoeij P 1998 VIERS-1 scatterometer model *J. Geophys. Res.* **103** 7807–31
- [26] Romeiser R, Alpers W and Wismann V 1997 An improved composite surface model for the radar backscattering cross section of the ocean surface: 1. Theory of the model and optimisation/validation by scatterometer data *J. Geophys. Res.* **102** 25 237–50
- [27] Lemaire D, Sobieski P and Guissard A 1999 Full-range sea surface spectrum in nonfully developed state for scattering calculations *IEEE Trans. Geosci. Remote Sens.* **37** 1038–51
- [28] Fuks I M 1966 Theory of radio wave scattering at a rough sea surface *Radiophys. Quantum Electron.* **9** 513–9
- [29] Valenzuela G R 1968 Scattering of electromagnetic waves from a tilted slightly rough surface *Radio Sci.* **3** 1057–66
- [30] Jackson F C, Walton W T, Hines D E, Walter B A and Peng C Y 1992 Sea surface mean square slope from K_u -band backscatter data *J. Geophys. Res.* **97** 11 411–27
- [31] Voronovich A G 1999 *Wave Scattering from Rough Surfaces* 2nd edn (Berlin: Springer) p 236
- [32] Voronovich A G 1994 Small-slope approximation for electromagnetic wave scattering at a rough interface of two dielectric half-spaces *Waves Random Media* **4** 337–67
- [33] Voronovich A G 2000 Small-slope approximation and two-scale model *Proc. Workshop Rough Surface Scattering and Related Phenomena (Napa Valley, Yountville, CA)* ed A A Maradudin (Irvine, CA: UC Irvine/Institute for Surface and Interface Science)
- [34] Elfouhaily T, Chapron B, Katsaros K and Vandemark D A 1997 Unified directional spectrum for long and short wind-driven waves *J. Geophys. Res.* **102** 15 781–96
- [35] Cox C and Munk W 1954 Measurement of the roughness of the sea surface from photographs of the sun's glitter *J. Opt. Soc. Am.* **44** 835–50
- [36] Cox C and Munk W 1954 Statistics of the sea surface derived from sun glitter *J. Mar. Res.* **13** 198–227
- [37] Dahl P H 1999 On bistatic sea surface scattering: field measurements and modeling *J. Acoust. Soc. Am.* **105** 2155–69

- [38] Brochat S L 1993 The small-slope approximation reflection coefficient for scattering from a Pierson–Moskowitz sea surface *IEEE Trans. Geosci. Remote Sens.* **31** 1112–4
- [39] Brochat S L and Thorsos E I 1997 An investigation of the small slope approximation for scattering from rough surfaces. Part II. Numerical studies *J. Acoust. Soc. Am.* **101** 2615–25
- [40] Yang T and Brochat S L 1992 A comparison of scattering model results for two-dimensional randomly rough surfaces *IEEE Trans. Antennas Propagat.* **40** 1505–12
- [41] Yang T and Brochat S L 1994 Acoustic scattering from a fluid–elastic-solid interface using the small slope approximation *J. Acoust. Soc. Am.* **96** 1796–804
- [42] Voronovich A G 1996 Non-local small-slope approximation for wave scattering from rough surfaces *Waves Random Media* **6** 151–67
- [43] Berman D H and Dacol D K 1990 Manifestly reciprocal scattering amplitudes for rough interface scattering *J. Acoust. Soc. Am.* **87** 2024–32
- [44] Voronovich A G, Zavorotny V U and Irisov V G 2000 Sea-roughness spectrum retrieval from radar and radiometric measurements *Proc. Int. Geosci. Remote Sensing Symp. (IGARSS-2000, Honolulu, HI)* vol VII, ed T I Stein (Piscataway, NJ: IEEE) pp 3102–4
- [45] Vandemark D, Chapron B, Walsh E J and Elfouhaily T 2000 Measurement and modeling of steep ocean wave slopes and absolute calibration of the radar altimeter *Proc. Int. Geosci. Remote Sensing Symp. (IGARSS-2000, Honolulu, HI, 2000)* vol IV, ed T I Stein (Piscataway, NJ: IEEE) pp 1495–7
- [46] Avanesova G G, Volyak K I and Shugan I V 1984 Measurements of wave characteristics by a side-looking airborne radar. Theory and experiment *Studies in Geophysics* (Moscow: Nauka) pp 94–123
- [47] Bunkin F V, Volyak K I and Shugan I V 1984 Statistics of speckle in radar images of the sea surface, recorded in horizontal polarization *Radiophys. Quantum Electron.* **27** 595–601
- [48] Phillips O M 1988 Radar returns from the sea surface—Bragg scattering and breaking waves *J. Phys. Oceanogr.* **18** 1065–74
- [49] Wetzel L B 1990 Electromagnetic scattering from the sea at low grazing angles *Surface Waves and Fluxes* vol II, ed G L Geernaert and W J Plant (Dordrecht: Kluwer) pp 109–71
- [50] Smirnov A V and Zavorotny V U 1995 Study of polarization differences in the Ku-band ocean radar imagery *J. Phys. Oceanogr.* **25** 2215–28
- [51] Quilfen Y, Chapron B, Bentamy A and Gourrion J 1999 Global ERS 1 and 2 NSCAT observations: upwind/cross-wind and upwind/downwind measurements *J. Geophys. Res.* **104** 11 459–69
- [52] Chapron B, Kerbaol V, Vandemark D and Elfouhaily T 2000 Importance of peakedness in sea slope measurements and applications *J. Geophys. Res.* **105** 17 195–202
- [53] Tatarskii V I and Tatarskii V V 1999 Statistical non-Gaussian model of sea surface with anisotropic spectrum for wave scattering theory *Progr. Electromagn. Res.* **25** 259–313
- [54] Omuircheartaigh I G and Monahan E C 1986 Statistical aspects of the relationship between oceanic whitecap coverage: wind speed and other environmental factors *Oceanic Whitecaps and Their Role in Air–Sea Exchange Process* ed E C Monahan and G MacNiocaill (Dordrecht: Reidel) pp 125–8
- [55] Komen G J, Cavaleri L, Donelan M, Hasselmann K, Hasselmann S and Janssen P A E M 1994 *Dynamics and Modelling of Ocean Waves* (Cambridge: Cambridge University Press) p 532